Massive MIMO precoder for long range in-band wireless backhaul

Alexis Bazin, Bruno Jahan, Maryline Hélard

RESEARCH

Massive MIMO precoder for long range in-band wireless backhaul

Alexis Bazin[1,2*], Bruno Jahan[1] and Maryline Hélard[2]

Abstract

Extending the coverage in low average revenue per user networks is a challenging task as the constraints are very high in terms of cost of deployment. In order to reduce this cost, part of the optical fiber classically used for the backhaul link can be replaced by a long range wireless link between two base stations. Additionally, an in-band communication, where the same frequency band is used for the access links and the backhaul link, avoids dispensing additional spectral resources. In this paper, a massive multiple-input multiple-output system combined with a new precoding technique is proposed to provide a long-range in-band wireless backhaul link, while controlling the interference on the user side induced by the in-band communication. The proposed precoder, called regularized zero forcing with controlled interference, is analytically compared with the maximum ratio transmission and the zero forcing precoders in terms of received power on the receiving base station and interference level on the user side. Thereby, this work proves that the proposed precoder outperforms the zero forcing precoder in terms of received power on the receiving base station side and limits the interference level on the user side unlike the maximum ratio transmission precoder. Simulation results confirm the analytical study over a realistic scenario.

Keywords: In-Band; Wireless Backhaul; Massive MIMO; Precoder; OFDM

1 Introduction

Mobile networks are constantly evolving and thus more and more people have access to the internet. The development of the fifth generation of cellular networks (5G) should boost this aspect. However, there are still inequalities regarding the ease of access to the internet [1]. In low average revenue per user (ARPU) areas, the deployment of the cellular network is by definition constrained by its cost, which slows down its development. In particular, the deployment of the links between the base stations (BSs) and the core network, the backhaul (BH) links, is an expensive task when using a classical optical fiber communication [2]. Nevertheless, a wireless link between two BSs, the first one acting as a relay for the second one, avoids the use of an optical fiber between the core network and the second BS. Thereby, this wireless BH link can be an appropriate solution to reduce the cost in low ARPU networks [2]. In particular, it should be a long range link of several kilometers

*Correspondence: alexis.bazin@insa-rennes.fr

[1]Department of Advanced Wireless Evolution, Orange Labs, 4 rue du Clos Courtel, 35512 Cesson-Sévigné, France

[2]Univ Rennes, INSA Rennes, CNRS, IETR (Institut d'Electronique et de Télécommunications de Rennes), UMR 6164, F-35000 Rennes, France

Full list of author information is available at the end of the article

and it should provide a sufficient data rate in order to maintain a good quality of service. Moreover, an adaptive link is preferable in order to counteract the damage caused by weather conditions. For example, the wind can move the antennas and can deflect the BH beam [3].

Radio-relay technologies are classical solutions to provide long-range wireless links of typically tens of kilometers [4]. These technologies are well-known since the first radio relay link was built in 1934 [4]. However, this solution is not adaptive and is more likely impacted by weather conditions (rain, temperature, wind, etc.). Moreover, even if some radio-relay technologies can achieve a data rate above 1 Gbps, their usual capabilities in terms of data rate are rather limited. Finally, a radio relay link requires a dedicated frequency band subject to regulation, which induces additional costs. For these reasons, radio-relay technologies may not be the best solutions for wireless BH in low ARPU areas.

In order to cover several kilometers, the use of sub-6 GHz frequencies seems to be appropriate since they experience lower path loss than higher frequencies. However, under 6 GHz the frequency resources are very scarce and expensive, which eliminates the possibility of using a dedicated frequency band for the BH. An interesting solution is therefore to use an in-band wireless BH, where the access links, between the BSs and the users, and the BH link use the same frequency band. The feasibility of such a solution was discussed in [5–10]. In these contributions, the authors multiplex the BH link and the access links in the time and frequency domains to avoid the spatial interference but at the price of a low spectral efficiency. They show that an in-band wireless BH is an interesting solution to improve the throughput of the cellular networks [5, 7–10] or to extend their coverage at a low cost [6].

Additionally, a massive multiple-input multiple-output (mMIMO) system with a relatively high number of antennas, especially on the BS side, is a popular trend for the development of 5G [11–13]. Indeed, combined with appropriate signal processing techniques, mMIMO systems offer a substantial number of advantages. On the transmitter side, they are able to focus the energy in the space domain [14, 15] and, on the receiver side, they can increase the signal-to-interference-plus-noise ratio (SINR) [16, 17]. More generally, mMIMO systems are interesting solutions to provide space-division multiple access (SDMA) and to improve the spectral and energy efficiency of the systems [18, 19]. For wireless BH, mMIMO techniques are suitable as they are adaptive solutions able to counteract the damage caused by weather conditions. Moreover, by improving the SINR on the receiver side, they can provide high data rates. The feasibility and challenges of mMIMO for wireless BH in 5G ultra dense networks was discussed in [20] in the context of millimeter waves communications. Additionally, in [20] the authors developed a new mMIMO hybrid precoding/combining scheme to provide point-to-multipoint wireless BH links. However, a dedicated frequency band is used for the BH link in [20].

Related Works: This paper considers an in-band wireless BH using a mMIMO system in order to multiplex the BH link and the access links in the space domain. This solution allows an increase of the spectral efficiency compared to these attained in [5–10]. Such a system has been recently studied in [21–25] for small cells deployment in 5G networks. In these studies, the BH links are deployed to serve small cell BSs inside the coverage of a macro cell.

- In [21], the authors proposed a mMIMO precoder on the BS side to provide an in-band wireless BH with the objective of maximizing the system throughput. Moreover, the mMIMO precoder

used on the BS side cancels the spatial interference on the small cell users.

- In [22], the mMIMO precoder used on the BS side is designed to simultaneously handle the access links for macro cell users and the BH links for small cell BSs. In parallel, a reverse time-division duplex (TDD) scheme is used in order to avoid the spatial interference. It means that the uplink of the small cells happens during the downlink of the macro cell, and vice versa.
- In [23] and [24], the mMIMO precoder on the BS side provides the BH links but does not control the potential spatial interference on the user side. Therefore, in order to improve the system capacity, they proposed a mix of in-band BH and out-of-band BH.
- In [25], the mMIMO precoder on the BS side simultaneously handles the access links for macro cell users and the BH links for small cell BSs but is also designed to suppress the spatial interference for small cell users.

All these studies could be extended to the case of a long-range in-band wireless BH link, where the BH link serves a neighboring macro cell. However, they are subject to the following limitations.

- On the one hand, regarding the long distance between the two considered BSs in low ARPU networks, a very directive BH link is required and the use of highly directive antennas is preferable for this BH link. On the other hand, the access links need to cover the entire macro-cell and the antennas should not be too directive for these access links. Therefore, using the same mMIMO antennas for the BH link and for the access links as in [22, 25] might not be adapted in the considered context.
- In general, the amount of data transmitted for the downlink is larger than the amount of data transmitted for the uplink. In a TDD scheme, it is thus preferable to have a longer time slot for the downlink than for the uplink. The reverse TDD scheme used in [22] imposes the same duration for the downlink and the uplink time slots. Therefore, the solution used in [22] is not suitable in the considered context and reduces the spectral efficiency of the system.
- Using the mix of in-band BH and out-of-band BH proposed in [23, 24] significantly reduces the spectral efficiency of the system as a dedicated frequency band is required for the out-of-band BH.
- The complete suppression of the interference on the user side as in [21, 25] induces a reduced received power on the receiving BS [14, 15]. This aspect is even more important regarding the long-range BH link studied in this paper.

Motivation and Contributions: In this paper, a new mMIMO precoding technique, easy to implement and called "regularized zero forcing with controlled interference" (RZF-CI), is introduced to provide a long-range in-band wireless BH link. The proposed precoder has to maximize the received power on the receiving BS, while limiting to a predetermined level the interference power on the users of the macro-cell, which are served in parallel. This study differs from [21–25] by the following points.

- Unlike in [22, 25], the mMIMO antenna arrays used in this paper are dedicated to the BH link and can be added on the top of the existing BSs. Thereby, these mMIMO antenna arrays can use highly directive antennas, which is necessary in order to optimize the gain of the BH link.
- The downlink of the BH link happens during the downlink of the access links. This solution is more adapted and more flexible than the reverse TDD scheme used in [22] as the time slot used for the

downlink can be longer than the time slot used for the uplink.

- The proposed RZF-CI precoder aims at controlling the interference on the user side unlike in [23, 24], when the in-band BH is considered.
- The proposed RZF-CI precoder controls but does not completely suppress the interference on the user side unlike in [21, 25]. Thereby, the received power on the receiving BS might be increased.

In order to evaluate the performance of the proposed RZF-CI precoder, an analytical comparison is carried out with the classical maximum ratio transmition (MRT) precoder [26], which maximizes the received power but does not control the interference on the user side as in [23, 24], when the in-band BH is considered. Moreover the RZF-CI precoder is also analytically compared with the zero forcing (ZF) precoder [27], which completely suppresses the interference on the user side as in [21, 25]. Finally, the performance of the proposed RZF-CI precoder is evaluated and compared to the MRT and the ZF precoders thanks to simulations for a realistic scenario using a geometry-based channel model.

Organization and Notations: The considered scenario is presented along with the system model in part 2. Based on this system model, the problem is defined in part 3. Then, the MRT and the ZF precoding techniques are presented in part 4 along with the proposed RZF-CI precoding technique. Moreover, in part 5.1 performance of these precoders are analytically compared. Simulation results are then given in part 5.2 in order to evaluate the performance of the RZF-CI precoding technique for a realistic scenario and to compare it to the performance of the MRT and ZF precoding techniques. Finally, a conclusion is drawn in the last part. The following notations are used in this paper. For a complex scalar, $|\,.\,|$ denotes the norm and $(\,.\,)^*$ denotes the complex conjugate. Moreover, vectors and matrices are represented in small boldface letters and capital boldface letters respectively. $(\,.\,)^T$ represents their transpose, $(\,.\,)^H$ represents their conjugate transpose and $\|\,.\,\|$ gives their Euclidean norm. Finally, $\mathbf{I}_N$ stands for the $(N \times N)$ identity matrix and $E[\,.\,]$ stands for the expected value.

2 Scenario and System Model

The aim of this paper is to study the deployment of an in-band BH link between two neighboring macro cells. Part 2.1 provides details regarding the considered scenario. Then, the system model is defined in parts 2.2, 2.3 and 2.4 respectively for the propagation channel, the transmitters and the receivers.

2.1 Considered Scenario

As described by Figure 1, this paper considers two neighboring macro-cells, the cell 1 and the cell 2, which are respectively served by the BS 1 and the BS 2. In particular, the user equipments (UEs) of the cell 1 (respectively the cell 2) are served by the BS 1 (respectively the BS 2) via the access links. These access links are represented in Figure 1 by the solid green arrows and are provided by dedicated antennas on the BS 1 and on the BS 2, which are further called access antennas in this paper. For the BH links between the core network and the two BSs, two schemes can be considered. On the one hand, in the classical wired BH scheme illustrated in Figure 1 (a), both the BS 1 and the BS 2 are connected to the core network via wired BH links. On the other hand, in the in-band wireless BH scheme illustrated in Figure 1 (b), the BS 1 is connected to the core network via a wired BH link and acts as a relay for the BS 2 via a wireless BH link between the BS 1 and the BS 2. This wireless BH link is represented in Figure 1 (b) by the solid red arrow and is created thanks to mMIMO antenna arrays added on the top of each BS, facing each other and further called BH antenna arrays. These mMIMO antenna arrays are

made of directive antennas and are thus adapted for the BH link as highlighted in the introduction. In this paper, the second scheme illustrated by Figure 1 (b) is considered as a potential solution to reduce the cost of deployment.

It is a known fact that the channel estimation process in a mMIMO system can be a complicated task when a Frequency-Division Duplex (FDD) scheme is considered [12, 18, 19]. Therefore, a TDD system, which takes advantage of the channel reciprocity, is preferable for the considered scenario and is assumed in this paper. Moreover, the uplink and the downlink for the cell 1, for the cell 2 and for the BH are assumed to be synchronized as in [21–25]. As highlighted in the introduction, the amount of data transmitted for the downlink is generally larger than the amount of data transmitted for the uplink. Therefore, unlike in [22], the same time slot is used for the downlink of the cell 1, the downlink of the cell 2 and the downlink of the BH, from the BS 1 to the BS 2. Similarly, the same time slot is used for the uplink of the cell 1, the uplink of the cell 2 and the uplink of the BH, from the BS 2 to the BS 1. This scheme is summarized by Figure 2, where the solid green arrows represent the access links and the solid red arrow represents the BH link.

The downlink of the considered TDD system is illustrated by Figure 2 (a). For the BH link, a beam is created between the BH antenna array of the BS 1 and the BH antenna array of the BS 2 thanks to a mMIMO precoding technique applied on the BH antenna array of the BS 1. However, this BH link uses the same frequency band as the access links and thus the secondary lobes of the created beam induce interfering signals between the BH antenna array of the BS 1 and part of the UEs. It is assumed in this paper that this interference is located near the BS 1 and thus only the UEs of the cell 1 are impacted. This assumption will be further verified through simulations in part 5.2. These interfering signals are represented by the dotted red arrows in Figure 2 (a). Additionally, the access antenna of the BS 2 sends data to the UEs of the cell 2, creating interfering signals on the BH antenna array of the BS 2. These interfering signals are represented by the dotted green arrow in Figure 2 (a).

The uplink of the considered scenario is illustrated by Figure 2 (b). For the BH link, a beam is created between the BH antenna array of the BS 2 and the BH antenna array of the BS 1 thanks to a mMIMO precoding technique used on the BH antenna array of the BS 2. This transmission creates interfering signals on the access antenna of the BS 2. These interfering signals are represented by the dotted red arrow in Figure 2 (b). Additionally, the UEs of the cell 1 send data to the access antenna of the BS 1, creating interfering signals on the BH antenna array of the BS 1. These interfering signals are represented by the dotted green arrow in Figure 2 (b).

As in [23–25], this paper does not study the overall TDD system but focuses on the downlink of the considered scenario described by Figure 2 (a). In particular, the mMIMO precoding technique used on the BH antenna array of the BS 1 is investigated. For the rest of this paper, an orthogonal frequency-division multiplexing (OFDM) modulation is used for the access and the BH links and the frequency-division multiple access (FDMA) method is used to serve the UEs for the access links. Moreover, each sub-carrier is independently processed and the focus is put on a particular sub-carrier. Finally, single-antenna UEs are considered in this paper for the sake of simplicity.

2.2 Propagation Channels

The propagation channel for the considered scenario can be divided in three parts:

- the useful channel, between the two BH antenna arrays,

- the interference channel, between the BH antenna array of the BS 1 and the UEs of the cell 1,
- the access channel, between the access antenna of the BS 1 and the UEs of the cell 1.

They are defined more thoroughly thereafter.

2.2.1 Useful Channel

The propagation channel between the N_t antennas of the first BH antenna array and the N_r antennas of the second BH antenna array is further called the useful channel in this paper. It can be described by the $(N_r \times N_t)$ matrix $\sqrt{P'_U}\mathbf{H}'_U$, where P'_U is the path loss between the BH antenna array of the BS 1 and the BH antenna array of the BS 2. Additionally, the matrix $\mathbf{H}'_U$ is defined by:

$$\mathbf{H}'_U = \left[\left(\mathbf{h}'^{0}_U\right)^T \quad \left(\mathbf{h}'^{1}_U\right)^T \quad \cdots \quad \left(\mathbf{h}'^{N_r-1}_U\right)^T \right]^T, \quad (1)$$

where:

$$\mathbf{h}'^{n_r}_U = \left[h'^{0,n_r}_U \quad h'^{1,n_r}_U \quad \cdots \quad h'^{N_t-1,n_r}_U \right] \quad (2)$$

is a $(1 \times N_t)$ vector with:

$$E\left[\left| h'^{n_t,n_r}_U \right|^2 \right] = 1, \ \forall (n_t, n_r) \in [0, N_t-1] \times [0, N_r-1]. \quad (3)$$

In particular, $\mathbf{h}'^{n_r}_U$ defines the propagation channel between the N_t transmit antennas and the receive antenna of index n_r.

An important particularity of the useful propagation channel studied in this paper is that it is mainly characterized by a long distance and by a strong line-of-sight (LOS) component. Thanks to theoretical studies and measurement campaigns [28–30], it is a known fact that, with such a LOS propagation channel, the received signals on the BH antenna array of the BS 2 can be seen as plane waves and the channel matrix $\mathbf{H}'_U$ can be assumed to be of rank-1. These particularities lead to the following statements.

- While this mMIMO system can improve the signal-to-noise ratio (SNR) thanks to its high number of antennas, with such a rank-1 channel matrix, no multiplexing gain can be expected.
- As the two BH antenna arrays are facing each other, the received plane waves are coplanar with the BH antenna array of the BS 2. Therefore, the propagation channel is considered to be the same whatever the receive antenna, meaning:

$$\mathbf{h}'^{n_r}_U = \mathbf{h}'^{n'_r}_U = \mathbf{h}_U \ \ \forall (n_r, n'_r) \in [0, N_r-1]^2. \quad (4)$$

According to these statements, the definition of the useful channel can be simplified. In particular, the system model does not consider the full mMIMO channel matrix $\mathbf{H}'_U$, but only the $(1 \times N_t)$ multiple-input single-output (MISO) channel vector $\mathbf{h}_U$:

$$\mathbf{h}_U = \left[h^0_U \quad h^1_U \quad \cdots \quad h^{N_t-1}_U \right], \quad (5)$$

with:

$$E\left[\left| h^{n_t}_U \right|^2 \right] = 1, \ \forall n_t \in [0, N_t-1]. \quad (6)$$

2.2.2 Interference Channel

As the FDMA method is used for the access links, at most one UE is impacted by the BH link on the considered sub-carrier. Moreover, as the UEs are equipped with a single antenna, the propagation channel between the BH antenna array of the BS 1 and the impacted UE is defined by a vector of size $(1 \times N_t)$ and denoted by $\sqrt{P_I}.\mathbf{h}_I$. P_I is the path loss of this channel and $\mathbf{h}_I$ is defined by:

$$\mathbf{h}_I = \left[h^0_I \quad h^1_I \quad \cdots \quad h^{N_t-1}_I \right], \quad (7)$$

with:

$$E\left[\left| h^{n_t}_I \right|^2 \right] = 1, \ \forall n_t \in [0, N_t-1]. \quad (8)$$

This propagation channel is further called the interference channel in this paper.

2.2.3 Access Channel

The propagation channel between the access antenna of the BS 1 and the impacted UE is further called the access channel in this paper. It is denoted by the complex scalar $\sqrt{P_{Acc}}.h_{Acc}$ with P_{Acc} the path loss of this channel and with:

$$E\left[|h_{Acc}|^2\right] = 1. \tag{9}$$

2.3 Transmitters

For the proposed scenario, two transmitters are considered: the BH antenna array of the BS 1 and the access antenna of the BS 1.

2.3.1 BH Antenna Array of the BS 1

As the channel matrix $\mathbf{H}'_U$ is a rank-1 channel matrix, only one symbol per channel use is sent from the BS 1 to the BS 2. In particular, on the considered sub-carrier, the data c of variance σ_c^2 is sent towards the BH antenna array of the BS 2. This transmission is realized using the precoder described by the vector $\mathbf{w}_U$ of size $(N_t \times 1)$. Therefore, the vector of precoded data is defined by:

$$\mathbf{x}_{BH} = \frac{\mathbf{w}_U}{\sqrt{\xi_w}}c, \tag{10}$$

where $\xi_w = \|\mathbf{w}_U\|^2$ is the power normalization factor, which is necessary to keep a total transmit power equal to σ_c^2.

2.3.2 Access Antenna of the BS 1

The access antenna of the BS 1 sends the data x_{Acc} dedicated to a UE of the cell 1. This transmission is assumed to be synchronous with the BH transmission.

2.4 Receivers

Two receivers are considered in the system: the BH antenna array of the BS 2 and the UE of the cell 1 served on the considered sub-carrier.

2.4.1 BH Antenna Array of the BS 2

On the BH antenna array of the BS 2, the received data on the antenna n_r coming from the BH antenna array of the BS 1 is, according to (4):

$$y_{BH}^{U,n_r} = \sqrt{P'_U}.\mathbf{h}_U.\mathbf{x}_{BH}. \tag{11}$$

Therefore, it comes:

$$y_{BH}^{U,n_r} = y_{BH}^{U,n'_r} \ \ \forall (n_r, n'_r) \in [0, N_r - 1]^2, \tag{12}$$

and the received useful signal is approximately the same whatever the considered receive antenna.

Additionally, there is an interference component coming from the access antenna of the BS 2. On the antenna n_r, this interference component is denoted by y_{BH}^{I,n_r}. Finally, the noise component on the antenna n_r is denoted by $b_{BH}^{n_r}$.

In this paper, the maximum ratio combining (MRC) technique is used on the BH antenna array of the BS 2 because of its low complexity, as explained thereafter. Indeed, it does not need to know the propagation channel between the access antenna of the BS 2 and the BH antenna array of the BS 2. Moreover, according to (12), the received useful signals on the BH antenna array of the BS 2 are similar whatever the considered antenna. Therefore, the received useful signals arrive consistently and the MRC combiner only consists in adding all the received signals in order to maximize the received useful power.

After adding all the received signals, the received data y_{BH} on the BH antenna array of the BS 2 is defined as follows:

$$y_{BH} = y_{BH}^{U} + y_{BH}^{I} + b_{BH}. \tag{13}$$

In (13), the noise component of variance $\sigma_{b,BH}^2$ is:

$$b_{BH} = \sum_{n_r=0}^{N_r-1} b_{BH}^{n_r}, \tag{14}$$

and the interference component coming from the access antenna of the BS 2 is:

$$y_{BH}^{I} = \sum_{n_r=0}^{N_r-1} y_{BH}^{I,n_r}. \quad (15)$$

Moreover, according to (11), the received useful signal coming from the BH antenna array of the BS 1 is:

$$\begin{aligned} y_{BH}^{U} = \sum_{n_r=0}^{N_r-1} y_{BH}^{U,n_r} &= N_r.\sqrt{P'_U}.\mathbf{h}_U.\mathbf{x}_{BH} \\ &= \sqrt{P_U}.\mathbf{h}_U.\mathbf{x}_{BH}, \end{aligned} \quad (16)$$

with:

$$P_U = N_r^2.P'_U. \quad (17)$$

Therefore, according to (10):

$$y_{BH}^{U} = \sqrt{P_U}\frac{\mathbf{h}_U\mathbf{w}_U}{\sqrt{\xi_w}}c. \quad (18)$$

In (16), the signals y_{BH}^{U,n_r} add up consistently, while the noise components $b_{BH}^{n_r}$ in (14) and the interference components y_{BH}^{I,n_r} in (15) add up in a non-consistent way. Thus, the MRC technique used in this paper allows increasing the SINR on the BH antenna array of the BS 2 for a very low complexity.

2.4.2 UE of cell 1

On the UE side, the UE antenna receives the useful data from the access antenna y_{Acc}^{U} defined as follows:

$$y_{Acc}^{U} = \sqrt{P_{Acc}}.h_{Acc}.x_{Acc}. \quad (19)$$

However, it also receives the interfering data y_{Acc}^{I} coming from the BH antenna array of the BS 1 and defined by:

$$y_{Acc}^{I} = \sqrt{P_I}.\mathbf{h}_I.\mathbf{x}_{BH}, \quad (20)$$

and thus, according to (10):

$$y_{Acc}^{I} = \sqrt{P_I}\frac{\mathbf{h}_I\mathbf{w}_U}{\sqrt{\xi_w}}c. \quad (21)$$

The received signal y_{Acc} is thus defined as follows:

$$y_{Acc} = y_{Acc}^{U} + y_{Acc}^{I} + b_{Acc}, \quad (22)$$

where b_{Acc} is the noise component of variance $\sigma_{b,Acc}^2 = \sigma_b^2$.

The system model for the considered scenario is illustrated by Figure 3.

3 Problem Statement

According to (22), the SNR on the UE side is defined by:

$$\rho = \frac{\left|y_{Acc}^{U}\right|^2}{\sigma_b^2}, \quad (23)$$

while the SINR is defined as follows:

$$\gamma = \frac{\left|y_{Acc}^{U}\right|^2}{\left|y_{Acc}^{I}\right|^2 + \sigma_b^2}. \quad (24)$$

In order to evaluate the damage caused by the BH link on the UE side, the metric Δ is defined as follows:

$$\Delta = \frac{\rho}{\gamma} = \frac{\left|y_{Acc}^{I}\right|^2 + \sigma_b^2}{\sigma_b^2} = 1 + \frac{\left|y_{Acc}^{I}\right|^2}{\sigma_b^2}, \quad (25)$$

or equivalently, according to (21):

$$\Delta = 1 + \frac{\left|\mathbf{h}_I\mathbf{w}_U\right|^2}{\xi_w}\frac{P_I\sigma_c^2}{\sigma_b^2}. \quad (26)$$

Therefore, $\Delta \geq 1$ and the higher the value of Δ, the bigger the detrimental impact of the BH link on the UE side.

In order to limit the damage caused by the BH link, the value Δ must be under a given value Δ_{max}. The value of Δ_{max} is set on the BS 1 side. It can be either small enough to consider a negligible impact of the BH link or chosen depending on the quality of service required for the impacted UE. As the system capacity on the UE side is equal to:

$$R_{UE} = E\left[\log_2\left(1+\gamma\right)\right], \quad (27)$$

keeping Δ under Δ_{max} induces a guaranteed minimum system capacity R_{UE}^{min} given by:

$$R_{UE}^{min} = \log_2\left(1 + \frac{1}{\Delta_{max}}\rho\right). \quad (28)$$

On the BH antenna array of the BS 2, the system capacity of the BH link is equal to:

$$R_{BH} = E\left[\log_2\left(1 + \frac{\left|y_{BH}^U\right|^2}{\left|y_{BH}^I\right|^2 + \left|b_{BH}\right|^2}\right)\right]. \quad (29)$$

While the precoder design has no impact on the interference power $|y_{BH}^I|^2$ or the noise power $|b_{BH}|^2$, it can increase the system capacity of the BH link R_{BH} by increasing the useful power $|y_{BH}^U|^2$. According to (18), the received useful power on the BS 2 is defined by:

$$\left|y_{BH}^U\right|^2 = P_U\sigma_c^2\frac{\left|\mathbf{h}_U\mathbf{w}_U\right|^2}{\xi_w}. \quad (30)$$

Moreover:

$$\left|y_{BH}^U\right|^2 \leq \left|\|\mathbf{h}_U\|.\frac{\|\mathbf{w}_U\|}{\sqrt{\xi_w}}\right|^2 P_U\sigma_c^2, \quad (31)$$

and as $(\|\mathbf{w}_U\|^2/\xi_w) = 1$, it comes:

$$\left|y_{BH}^U\right|^2 \leq P_U\|\mathbf{h}_U\|^2\sigma_c^2. \quad (32)$$

The problem addressed in this paper can therefore be posed as follows:

$$\begin{array}{ll}\underset{\mathbf{w}_U\in\mathbb{C}^{N_t}}{\text{maximize}} & \left|y_{BH}^U\right|^2 \\ \text{subject to} & \Delta \leq \Delta_{max}.\end{array} \quad (33)$$

Equivalently, using (30), (26) and as $\xi_w = \|\mathbf{w}_U\|^2$, the problem (33) is equivalent to:

$$\begin{array}{ll}\underset{\mathbf{w}_U\in\mathbb{C}^{N_t}}{\text{maximize}} & \frac{\left|\mathbf{h}_U\mathbf{w}_U\right|^2}{\|\mathbf{w}_U\|^2} \\ \text{subject to} & \frac{\left|\mathbf{h}_I\mathbf{w}_U\right|^2}{\|\mathbf{w}_U\|^2} \leq \frac{\sigma_b^2}{P_I\sigma_c^2}\left(\Delta_{max} - 1\right).\end{array} \quad (34)$$

By setting $\mathbf{w}'_U = \mathbf{w}_U/\|\mathbf{w}_U\|$, the problem (34) can be rewritten as follows:

$$\begin{array}{ll}\underset{\mathbf{w}'_U\in\mathbb{C}^{N_t}}{\text{minimize}} & -\left|\mathbf{h}_U\mathbf{w}'_U\right|^2 \\ \text{subject to} & \left|\mathbf{h}_I\mathbf{w}'_U\right|^2 \leq \frac{\sigma_b^2}{P_I\sigma_c^2}\left(\Delta_{max} - 1\right) \\ \text{and} & \|\mathbf{w}'_U\|^2 = 1.\end{array} \quad (35)$$

In the problem (35), the objective function $-|\mathbf{h}_U\mathbf{w}'_U|^2$ is a concave function, the function $|\mathbf{h}_I\mathbf{w}'_U|^2$ in the inequality constraint is a convex function and the function $\|\mathbf{w}'_U\|^2$ in the equality constraint is a convex function. To the best of the authors' knowledge, the problem (35) does not describe a classical optimization problem and, in particular, is a non-convex optimization problem [31]. In this paper, we decide to simplify this problem. To this end, the use of a regularized zero forcing (RZF) precoding structure is proposed in the next part as in [27].

4 Precoding Techniques

The presented precoding techniques are derived from the multi-user multiple-input multiple-output (MU-MIMO) precoding matrices defined in [15, 27]. Indeed, our system can be seen as a MU-MIMO system with 2 users, where the data $c_{BH} = c$ is sent to the BH antenna array of the BS 2 and the data $c_{UE} = 0$ is sent to the UE. The $(N_t \times 2)$ precoding matrix $\mathbf{W}$ is defined as follows:

$$\mathbf{W} = \begin{bmatrix}\mathbf{w}_U & \mathbf{w}_I\end{bmatrix}, \quad (36)$$

with $\mathbf{w}_I$ being the $(N_t \times 1)$ precoding vector intended to send the data c_{UE}. Additionally, the $(2 \times N_t)$ channel matrix $\mathbf{H}$ is described as follows:

$$\mathbf{H} = \begin{bmatrix}\mathbf{h}_U^T & \mathbf{h}_I^T\end{bmatrix}^T. \quad (37)$$

Finally, the correlation factor Γ_h is defined by:

$$\Gamma_h = \frac{\mathbf{h}_I}{\|\mathbf{h}_I\|}\frac{\mathbf{h}_U^H}{\|\mathbf{h}_U\|}, \quad (38)$$

and thus $0 \leq |\Gamma_h| \leq 1$. This correlation factor reflects the correlation between the useful channel $\mathbf{h}_U$ and the interference channel $\mathbf{h}_I$ so that the higher the value of $|\Gamma_h|$, the higher the correlation between $\mathbf{h}_U$ and $\mathbf{h}_I$.

In this part, three precoding techniques are introduced: the MRT and ZF precoders as well as the proposed RZF-CI precoder.

4.1 Maximum Ratio Transmission (MRT)

The MRT precoder [26] is intended to maximize the received power without controlling the multi-user interference, as in [23, 24]. It is defined as follows for MU-MIMO systems:

$$\mathbf{W} = \mathbf{H}^H. \tag{39}$$

As $\xi_w = \|\mathbf{w}_U\|^2$ and according to (36) and (37), the precoding vector for wireless BH can be written as follows:

$$\begin{cases} \mathbf{w}_U &= \dfrac{\mathbf{h}_U^H}{\|\mathbf{h}_U\|}, \\ \xi_w &= 1. \end{cases} \tag{40}$$

4.2 Zero Forcing (ZF)

The ZF precoder is designed to suppress the multi-user interference, as in [21, 25], and is defined by the following matrix:

$$\mathbf{W} = \mathbf{H}^H \left(\mathbf{H}\mathbf{H}^H\right)^{-1}, \tag{41}$$

for MU-MIMO systems. The inversion of a (2×2) matrix $\mathbf{A}$ gives:

$$\mathbf{A}^{-1} = \frac{1}{det(\mathbf{A})} adj(\mathbf{A}), \tag{42}$$

where $det(\mathbf{A})$ is the determinant of $\mathbf{A}$ and $adj(\mathbf{A})$ is the adjugate matrix of $\mathbf{A}$. Therefore, according to (37) and (38), it simply comes:

$$\begin{aligned} \mathbf{H}\mathbf{H}^H &= \begin{bmatrix} \|\mathbf{h}_U\|^2 & \left(\mathbf{h}_I \mathbf{h}_U^H\right)^* \\ \mathbf{h}_I \mathbf{h}_U^H & \|\mathbf{h}_I\|^2 \end{bmatrix} \\ &= \|\mathbf{h}_U\| \, \|\mathbf{h}_I\| \begin{bmatrix} \dfrac{\|\mathbf{h}_U\|}{\|\mathbf{h}_I\|} & \Gamma_h^* \\ \Gamma_h & \dfrac{\|\mathbf{h}_I\|}{\|\mathbf{h}_U\|} \end{bmatrix}, \end{aligned} \tag{43}$$

and (42) gives:

$$\begin{aligned} \left(\mathbf{H}\mathbf{H}^H\right)^{-1} &= \frac{\|\mathbf{h}_U\| \, \|\mathbf{h}_I\|}{det\left(\mathbf{H}\mathbf{H}^H\right)} \begin{bmatrix} \dfrac{\|\mathbf{h}_I\|}{\|\mathbf{h}_U\|} & -\Gamma_h^* \\ -\Gamma_h & \dfrac{\|\mathbf{h}_U\|}{\|\mathbf{h}_I\|} \end{bmatrix} \\ &= \frac{\|\mathbf{h}_U\| \, \|\mathbf{h}_I\|^2}{det\left(\mathbf{H}\mathbf{H}^H\right)} \begin{bmatrix} \dfrac{1}{\|\mathbf{h}_U\|} & -\dfrac{\Gamma_h^*}{\|\mathbf{h}_I\|} \\ -\dfrac{\Gamma_h}{\|\mathbf{h}_I\|} & \dfrac{\|\mathbf{h}_U\|}{\|\mathbf{h}_I\|^2} \end{bmatrix}. \end{aligned} \tag{44}$$

Therefore, as $\xi_w = \|\mathbf{w}_U\|^2$ and according to (36) and (37), the precoding vector for wireless BH can be written as follows:

$$\begin{cases} \mathbf{w}_U &= \dfrac{\mathbf{h}_U^H}{\|\mathbf{h}_U\|} - \Gamma_h \dfrac{\mathbf{h}_I^H}{\|\mathbf{h}_I\|}, \\ \xi_w &= 1 - |\Gamma_h|^2. \end{cases} \tag{45}$$

One can see that the complexity is low for wireless BH transmissions as no matrix inversion is needed.

4.3 Regularized Zero Forcing with Controlled Interference (RZF-CI)

The proposed RZF-CI precoder is based on the RZF matrix structure, which is defined by:

$$\mathbf{W} = \mathbf{H}^H \left(\mathbf{H}\mathbf{H}^H + \alpha' \mathbf{I}_2\right)^{-1}, \tag{46}$$

with $\alpha' \in \mathbb{R}^+$, for MU-MIMO systems. On the one hand, when $\alpha' \to +\infty$ the RZF precoder is equivalent to a MRT precoder. On the other hand, when $\alpha' = 0$ the RZF precoder is equivalent to a ZF precoder. Therefore, the RZF precoder structure allows reaching a trade-off between the MRT precoder and

the ZF precoder. According to (37) and (38), it comes:

$$\begin{aligned}&\mathbf{H}\mathbf{H}^H+\alpha'\mathbf{I}_2\\&=\begin{bmatrix}\|\mathbf{h}_U\|^2+\alpha' & \left(\mathbf{h}_I\mathbf{h}_U^H\right)^*\\ \mathbf{h}_I\mathbf{h}_U^H & \|\mathbf{h}_I\|^2+\alpha'\end{bmatrix}\\&=\|\mathbf{h}_U\|\|\mathbf{h}_I\|\begin{bmatrix}\frac{\|\mathbf{h}_U\|^2+\alpha'}{\|\mathbf{h}_U\|\|\mathbf{h}_I\|} & \Gamma_h^*\\ \Gamma_h & \frac{\|\mathbf{h}_I\|^2+\alpha'}{\|\mathbf{h}_U\|\|\mathbf{h}_I\|}\end{bmatrix}.\end{aligned}\tag{47}$$

Therefore, (42) gives:

$$\begin{aligned}&\left(\mathbf{H}\mathbf{H}^H+\alpha'\mathbf{I}_2\right)^{-1}\\&=\frac{\|\mathbf{h}_U\|\|\mathbf{h}_I\|}{det\left(\mathbf{H}\mathbf{H}^H+\alpha'\mathbf{I}_2\right)}\begin{bmatrix}\frac{\|\mathbf{h}_I\|^2+\alpha'}{\|\mathbf{h}_U\|\|\mathbf{h}_I\|} & -\Gamma_h^*\\ -\Gamma_h & \frac{\|\mathbf{h}_U\|^2+\alpha'}{\|\mathbf{h}_U\|\|\mathbf{h}_I\|}\end{bmatrix},\end{aligned}\tag{48}$$

or equivalently:

$$\begin{aligned}&\left(\mathbf{H}\mathbf{H}^H+\alpha'\mathbf{I}_2\right)^{-1}=\frac{\|\mathbf{h}_U\|\|\mathbf{h}_I\|^2}{det\left(\mathbf{H}\mathbf{H}^H+\alpha'\mathbf{I}_2\right)}\\&\times\begin{bmatrix}\frac{1}{\|\mathbf{h}_U\|}\left(1+\frac{\alpha'}{\|\mathbf{h}_I\|^2}\right) & -\frac{\Gamma_h^*}{\|\mathbf{h}_I\|}\\ -\frac{\Gamma_h}{\|\mathbf{h}_I\|} & \frac{\|\mathbf{h}_U\|}{\|\mathbf{h}_I\|^2}\left(1+\frac{\alpha'}{\|\mathbf{h}_U\|^2}\right)\end{bmatrix}.\end{aligned}\tag{49}$$

Therefore, as $\xi_w=\|\mathbf{w}_U\|^2$ and according to (36) and (37), the precoding vector for wireless BH can be written as follows:

$$\begin{cases}\mathbf{w}_U &= (1+\alpha)\frac{\mathbf{h}_U^H}{\|\mathbf{h}_U\|}-\Gamma_h\frac{\mathbf{h}_I^H}{\|\mathbf{h}_I\|},\\ \xi_w &= (1+\alpha)^2-2(1+\alpha)|\Gamma_h|^2+|\Gamma_h|^2,\end{cases}\tag{50}$$

with:

$$\alpha=\frac{\alpha'}{\|\mathbf{h}_I\|^2},\tag{51}$$

$\alpha\in\mathbb{R}^+$. With this RZF structure, the received useful power on the second BH antenna array $|y_{BH}^U|^2$, defined in (30), and the metric Δ, defined in (26), are now function of the variable α. Therefore, $|y_{BH}^U|^2$ and Δ become $|y_{BH}^U(\alpha)|^2$ and $\Delta(\alpha)$.

The RZF structure provides a degree of freedom with the variable α. Based on the RZF structure described before, the proposed RZF-CI precoder exploits this degree of freedom. It uses the optimal value of α to maximize the received power on the receiving BS, while keeping the interference power on the UE side under a given power level. In particular, the value of α is chosen to solve the following problem:

$$\begin{aligned}&\underset{\alpha\in\mathbb{R}^+}{\text{maximize}} && \left|y_{BH}^U(\alpha)\right|^2\\&\text{subject to} && \Delta(\alpha)\leq\Delta_{max}.\end{aligned}\tag{52}$$

The variable Δ_∞ is defined as follows:

$$\Delta_\infty=\Delta(\alpha\to+\infty)=1+|\Gamma_h|^2P_I\|\mathbf{h}_I\|^2\frac{\sigma_c^2}{\sigma_b^2}.\tag{53}$$

Δ_∞ corresponds to the value of Δ when the MRT precoder is used and it can be computed on the UE side during a preliminary step and sent to the BS 1 during the uplink. Additionally, the variable α_0 is defined as follows:

$$\alpha_0=\frac{\left(1-|\Gamma_h|^2\right)+\sqrt{\left(1-|\Gamma_h|^2\right)\left(\frac{\Delta_\infty-1}{\Delta_{max}-1}-|\Gamma_h|^2\right)}}{\frac{\Delta_\infty-1}{\Delta_{max}-1}-1}.\tag{54}$$

This value can be computed by knowing the values of Δ_{max}, Δ_∞ and $|\Gamma_h|^2$.

Appendix A shows that the problem (52) is easier to solve than the problem (33), as the variable to be optimized is the real positive scalar α instead of the complex vector $\mathbf{w}_U$. Moreover, Appendix A also gives the optimal solution of the problem (52). In particular, it gives the following structure for the RZF-CI precoder if $\Delta_\infty\leq\Delta_{max}$:

$$\begin{cases}\mathbf{w}_U &= \frac{\mathbf{h}_U^H}{\|\mathbf{h}_U\|},\\ \xi_w &= 1,\end{cases}\tag{55}$$

and, if $\Delta_\infty > \Delta_{max}$:

$$\begin{cases} \mathbf{w}_U &= (1+\alpha_0)\dfrac{\mathbf{h}_U^H}{\|\mathbf{h}_U\|} - \Gamma_h \dfrac{\mathbf{h}_I^H}{\|\mathbf{h}_I\|}, \\ \xi_w &= (1+\alpha_0)^2 - 2(1+\alpha_0)|\Gamma_h|^2 + |\Gamma_h|^2. \end{cases} \tag{56}$$

One can see that $\mathbf{w}_U$ is equivalent to a MRT precoder when $\Delta_{max} \geq \Delta_\infty$ and to a ZF precoder when Δ_{max} is set to its minimum value 1. Moreover, the complexity of the RZF-CI precoder is slightly increased compared to this of the ZF precoder defined in (45) but remains low as no matrix inversion is needed.

5 Results and Discussion

In part 5.1 performance of the three precoders defined previously are analytically compared. Simulation results are then given in part 5.2 in order to evaluate performance of these precoding techniques for a realistic scenario.

5.1 Analytical Results

The performance of the studied precoders, defined in the previous part, are now analytically compared in terms of received useful power on the BH antenna array of the BS 2 and of interference power on the UE side.

Proposition 1 *With the MRT precoder, the received useful power on the BH antenna array of the BS 2 is maximized and equal to:*

$$\left|y_{BH}^U\right|^2 = P_U \left\|\mathbf{h}_U\right\|^2 \sigma_c^2. \tag{57}$$

However, the interference on the UE side is not controlled and thus this precoding technique might not fulfill the condition $\Delta \leq \Delta_{max}$.

Proof Using (40) in (30) directly leads to (57). This is the maximum value for the received useful power on the receiving BS according to (32). Moreover, using (40) in (26), it comes:

$$\Delta = \Delta_\infty = 1 + |\Gamma_h|^2 P_I \left\|\mathbf{h}_I\right\|^2 \frac{\sigma_c^2}{\sigma_b^2}. \tag{58}$$

Therefore, the condition $\Delta \leq \Delta_{max}$ is fulfilled only if:

$$|\Gamma_h|^2 \leq (\Delta_{max} - 1)\, \frac{\sigma_b^2}{P_I \left\|\mathbf{h}_I\right\|^2 \sigma_c^2}. \tag{59}$$

□

Proposition 2 *With the ZF precoder, the received useful power on the BH antenna array of the BS 2 is equal to:*

$$\left|y_{BH}^U\right|^2 = P_U \left\|\mathbf{h}_U\right\|^2 \sigma_c^2 \times \left(1 - |\Gamma_h|^2\right), \tag{60}$$

and is maximized only if $|\Gamma_h| = 0$. Additionally, the value of Δ is minimized and thus the condition $\Delta \leq \Delta_{max}$ is always fulfilled.

Proof using (45) and (38) in (30), the received useful power on the BH antenna array of the BS 2 is equal to:

$$\begin{aligned} \left|y_{BH}^U\right|^2 &= P_U \sigma_c^2 \frac{\left|\|\mathbf{h}_U\| - |\Gamma_h|^2 \left\|\mathbf{h}_U\right\|\right|^2}{1 - |\Gamma_h|^2} \\ &= P_U \left\|\mathbf{h}_U\right\|^2 \sigma_c^2 \times \frac{\left|1 - |\Gamma_h|^2\right|^2}{1 - |\Gamma_h|^2} \\ &= P_U \left\|\mathbf{h}_U\right\|^2 \sigma_c^2 \times \left(1 - |\Gamma_h|^2\right). \end{aligned} \tag{61}$$

According to (32), the received useful power on the BS 2 is maximized only if $|\Gamma_h| = 0$. Moreover, using (45) in (26), it comes:

$$\Delta = 1 + \frac{\left|\mathbf{h}_I \left(\mathbf{h}_U^H/\|\mathbf{h}_U\| - \Gamma_h \mathbf{h}_I^H/\|\mathbf{h}_I\|\right)\right|^2}{1 - |\Gamma_h|^2} \frac{P_I \sigma_c^2}{\sigma_b^2}. \tag{62}$$

According to (38), it comes:

$$\Delta = 1 + \frac{\left|\left(\|\mathbf{h}_I\|\,\Gamma_h - \|\mathbf{h}_I\|\,\Gamma_h\right)\right|^2}{1 - |\Gamma_h|^2} \frac{P_I \sigma_c^2}{\sigma_b^2} = 1. \tag{63}$$

Therefore, Δ is equal to its minimum value. □

Proposition 3 *With the RZF-CI precoder, the received useful power on the BH antenna array of the BS 2 is equal to:*

$$\left|y_{BH}^{U}\right|^2 = \begin{cases} P_U \left\|\mathbf{h}_U\right\|^2 \sigma_c^2 & \text{if} \quad \Delta_\infty \leq \Delta_{max}, \\ P_U \left\|\mathbf{h}_U\right\|^2 \sigma_c^2 \left(1 - \varepsilon.|\Gamma_h|^2\right) & \text{if} \quad \Delta_\infty > \Delta_{max}, \end{cases} \tag{64}$$

with:

$$\varepsilon = \left(1 + 2\alpha_0 + \frac{\alpha_0^2}{1 - |\Gamma_h|^2}\right)^{-1}, \tag{65}$$

and with:

$$0 \geq \varepsilon \geq 1. \tag{66}$$

Therefore, the received useful power with the RZF-CI precoder is always higher or equal to the received useful power with the ZF precoder. Additionally, the condition $\Delta \leq \Delta_{max}$ *is always fulfilled.*

Proof Appendix B provides the detailed theoretical derivation of the expression of the received useful power with the RZF-CI precoder. Moreover, The RZF-CI precoder is designed to fulfill the condition $\Delta \leq \Delta_{max}$ as explained in part 4.3. □

Based on these theoretical results, Figure 4 gives the theoretical received power on the BS 2 with the MRT, the ZF and the proposed RZF-CI precoders as a function of the correlation factor Γ_h and of the ratio $(\Delta_\infty - 1)/(\Delta_{max} - 1)$ for the RZF-CI precoder. This ratio can be seen as the amount of interference to suppress as it increases when the impact of the BH link on the UE side increases, meaning when Δ_∞ increases and decreases when the limit Δ_{max} increases. As expected, the RZF-CI precoder is a trade-off between the MRT precoder, comparable to those used in [23, 24], and the ZF precoder, similar to the precoders used in [21, 25]. Moreover, the received power with the RZF-CI precoder increases when the ratio $(\Delta_\infty - 1)/(\Delta_{max} - 1)$ decreases, meaning when the amount of interference to suppress decreases.

Table 1 Simulation Parameters

FFT size	1024
Inter-carrier spacing	15 kHz
CP length	4.7 μs
Center frequency	4 GHz
BH antenna arrays: number of antennas per column	16
BH antenna arrays: number of antennas per line	4
BH antenna arrays: inter-antenna spacing	10 cm
BH antenna arrays: half-power beamwidth	30°
BH antenna arrays: height	35 m
Distance between the BS 1 and the BS 2	10 km
UE: height	1.5 m

5.2 Simulation Results

In order to numerically evaluate the performance of the RZF-CI precoder, the QuaDRiGa 3D channel simulator [32, 33] is used in this part to simulate geometry-based channel models. The simulations thus take into account the geometry of the propagation environment and the correlation between the antennas, which is important as the correlation factor Γ_h depends on these aspects and has a significant impact on the performance of the system as shown in the previous part. The BH antenna arrays are identical uniform rectangular arrays facing each other and the channel model used between these two antenna arrays is the 3GPP 38.901 rural macro-cell (RMa) LOS spatial channel model [34]. Moreover, the considered UE is equipped with an omni-directional antenna, is located on the straight line joining the BS 1 and the BS 2 and the 3GPP 38.901 RMa LOS spatial channel model is also used between the BS 1 and this UE. This configuration corresponds to the worst case for the UE, which might be highly impacted by the BH link. For the sake of simplicity, a perfect channel estimation is assumed. The simulation parameters are given by Table 1.

The normalized interference power on the UE side is first drawn in Figure 5 as a function of the distance between the BS 1 and the UE when the MRT precoder is used. This Figure shows that the secondary lobes of the created beam induce interference peaks with a significant power when the distance between the BS 1 and the UE is below 1 km. After 1 km, the path loss induces a reduction of the interference power, which constantly decreases and loses more than 20 dB at a distance of 5 km. Therefore, and in accordance with preliminary assumptions described in part 2, the interference on the UE side is predominant for UEs located near the BS 1.

The bit error rate (BER) on the UE side is then computed as a function of the SNR when the MRT, the ZF and the RZF-CI precoders (with $\Delta_{max} = 0.5\ dB$ and $\Delta_{max} = 1\ dB$) are used. The distance between the BS 1 and the UE is set to 2 km. The results are given by Figure 6. The interference on the UE side is canceled using the ZF precoder, which experiences the best results in terms of BER on the UE side. Conversely, the interference on the UE side highly impacts the BER when the MRT precoder is used as it does not control this interference. Therefore, to reach a BER of 10^{-2} when the MRT precoder is used, the UE needs a SNR greater than 20 dB while only 14.5 dB is necessary when the ZF precoder is used. As the interference level is high for a UE at this position, the value of Δ_{∞} is greater than Δ_{max}. Therefore, in Figure 6 the curves for the proposed RZF-CI precoder are shifted versions of the ZF curve with a shift equal to the value of Δ_{max}. As expected, the performance of the RZF-CI precoder is thus slightly worse than this of the ZF precoder but remains under control.

The normalized received useful power on the BS 2 $|y_{BH}^{U}|^2 \ / \ (P_U \left\|\mathbf{h}_U\right\|^2 \sigma_c^2)$ is now computed as a function of the distance between the BS 1 and the UE when the MRT, the ZF and the RZF-CI precoders (with $\Delta_{max} = 0.5\ dB$ and $\Delta_{max} = 1\ dB$) are used. The results are given by Figure 7. On the one hand, while the MRT precoder offers poor performance in terms of BER on the UE side, it always maximizes the received useful power on the BS 2. On the other hand, the good performance of the ZF precoder in terms of BER on the UE side is balanced by the high loss in terms of received useful power on the BS 2. Therefore, a loss of almost 8 dB can occur, compared to the received useful power reached by the MRT precoder, when the UE is at the cell-edge. As expected, the RZF-CI precoding technique outperforms the ZF precoding technique in terms of received useful power on the BS 2. Moreover, this result is consistent with the theoretical results as the higher the value of Δ_{max}, the higher the received useful power on the BS 2. Finally, the loss of received useful power is very limited compared to the received useful power reached by the MRT precoder. The RZF-CI precoder looses at most 1.5 dB when $\Delta_{max} = 0.5\ dB$ and 1 dB when $\Delta_{max} = 1\ dB$.

To conclude, the proposed RZF-CI precoding technique appears to be a good trade-off between the MRT and the ZF precoding techniques used in the literature [21, 23–25]. By choosing the value of Δ_{max}, the performance in terms of BER on the UE side is controlled and the loss of received useful power on the BS 2 remains limited. Therefore, the simulations highlight the superiority of the proposed solution compared to the MRT and ZF precoders without leading to an excessive complexity.

6 Conclusion

A new mMIMO precoder called RZF-CI is proposed in this paper. This precoder is intended to provide a long-range in-band wireless BH link between two BSs. The particularity of the RZF-CI precoder is its ability to control the interference on the UE side, unlike the classical MRT precoder so that a minimum capacity is guaranteed for each UE. Moreover, in this paper,

an analytical study proved that the proposed solution always outperforms the ZF precoder used in the literature in terms of received power on the receiving BS and thus allows a higher system capacity for the BH link.

The simulations conducted in this paper highlight the benefits of this novel precoding technique. In terms of BER on the UE side, the degradation is controlled with the proposed RZF-CI precoder, while the performance with the MRT precoder is highly impacted by the in-band communication. In terms of received useful power on the receiving BS, the RZF-CI precoder allows an important gain compared with the ZF precoder (up to 8 dB), while the loss of power is rather limited compared with the MRT precoder (up to 1.5 dB).

By combining the flexibility and the low complexity of the new RZF-CI precoder with the advantages of having an in-band wireless BH link, the proposed solution is a cheap and effective way to extend the coverage of the cellular networks and to improve the quality of service in low ARPU networks.

Further studies could complete this contribution. Firstly, on the BH antenna array of the BS 2, other combining techniques could be studied. For example, a ZF technique canceling the interference coming from access antenna of the BS 2 or a minimum mean square error (MMSE) technique providing a trade-off between the MRC and the ZF techniques. Moreover, this paper focused on the downlink of a TDD system, but the uplink of the proposed system can be investigated in order to cope with the interference induced in this context (see Figure 2 (b)). Finally, the FDMA method is considered in this study to separate the UEs. However, it would be interesting to extend this work with MU-MIMO systems, where multiple UEs share the same frequency-time resources.

7 Methods/Experimental

The aim of this work is to design a new mMIMO precoder for long-range in-band wireless BH. To this end, a RZF structure is used and the optimization problem defined in (52) is solved accordingly. Simulations are then conducted using Matlab and the QuaDRiGa 3D channel simulator [32, 33].

Appendix A: Solution of the Problem (52)

Using (50) in (30), it comes:

$$\begin{aligned}&\left|y_{BH}^{U}(\alpha)\right|^2\\&\quad= P_U\sigma_c^2\frac{\left|(1+\alpha)\left\|\mathbf{h}_U\right\|-|\Gamma_h|^2\left\|\mathbf{h}_U\right\|\right|^2}{\left((1+\alpha)-|\Gamma_h|^2\right)^2+|\Gamma_h|^2-|\Gamma_h|^4}\\&\quad= P_U\left\|\mathbf{h}_U\right\|^2\sigma_c^2\frac{\left((1+\alpha)-|\Gamma_h|^2\right)^2}{\left((1+\alpha)-|\Gamma_h|^2\right)^2+|\Gamma_h|^2-|\Gamma_h|^4},\end{aligned}\tag{67}$$

and:

$$\begin{aligned}\left|y_{BH}^{U}(\alpha)\right|^2&= P_U\left\|\mathbf{h}_U\right\|^2\sigma_c^2\\&\quad\times\left(1-\frac{|\Gamma_h|^2\left(1-|\Gamma_h|^2\right)}{\left(1+\alpha-|\Gamma_h|^2\right)^2+|\Gamma_h|^2\left(1-|\Gamma_h|^2\right)}\right).\end{aligned}\tag{68}$$

Therefore, as $0\leq|\Gamma_h|^2\leq 1$, the value of $\left|y_{BH}^{U}(\alpha)\right|^2$ increases with the increase of α and is thus an increasing function.

Additionally, using (50) in (26), it comes:

$$\begin{aligned}&\Delta(\alpha)\\&=1+\frac{P_I\sigma_c^2}{\sigma_b^2}\frac{|(1+\alpha)\Gamma_h\left\|\mathbf{h}_I\right\|-\Gamma_h\left\|\mathbf{h}_I\right\||^2}{(1+\alpha)^2-2(1+\alpha)|\Gamma_h|^2+|\Gamma_h|^2}\\&=1+P_I\left\|\mathbf{h}_I\right\|^2\frac{\sigma_c^2}{\sigma_b^2}\frac{\alpha^2|\Gamma_h|^2}{\alpha^2+2(1-|\Gamma_h|^2)\alpha+(1-|\Gamma_h|^2)}\\&=1+P_I\left\|\mathbf{h}_I\right\|^2\frac{\sigma_c^2}{\sigma_b^2}\frac{|\Gamma_h|^2}{1+2(1-|\Gamma_h|^2)\frac{1}{\alpha}+(1-|\Gamma_h|^2)\frac{1}{\alpha^2}}.\end{aligned}\tag{69}$$

As $0\leq|\Gamma_h|^2\leq 1$, the value of $\Delta(\alpha)$ also increases with the increase of α and is thus an increasing function.

Let us define the variable Δ_∞ as follows:

$$\Delta_\infty=\Delta(\alpha\to+\infty)=1+|\Gamma_h|^2P_I\left\|\mathbf{h}_I\right\|^2\frac{\sigma_c^2}{\sigma_b^2}.\tag{70}$$

If $\Delta_\infty \leq \Delta_{max}$, the value of $\left|y_{BH}^U(\alpha)\right|^2$ is not limited by the value of $\Delta(\alpha)$ and can reach its maximum value when $\alpha \to +\infty$. If $\Delta_\infty > \Delta_{max}$, the value of $\left|y_{BH}^U(\alpha)\right|^2$ is limited by the value of $\Delta(\alpha)$. As both $\left|y_{BH}^U(\alpha)\right|^2$ and $\Delta(\alpha)$ are increasing functions, the problem (52) is solved in this context when $\Delta(\alpha) = \Delta_{max}$. Therefore, the optimal value for α is:

$$\alpha = \begin{cases} +\infty & \text{if} \quad \Delta_\infty \leq \Delta_{max}, \\ \alpha_0 & \text{if} \quad \Delta_\infty > \Delta_{max}, \end{cases} \tag{71}$$

α_0 being the positive solution of the equation $\Delta(\alpha) = \Delta_{max}$. This equality is equivalent to:

$$\Delta(\alpha) - 1 = \Delta_{max} - 1, \tag{72}$$

or, using (70) in (69):

$$\frac{\alpha^2}{\alpha^2 + 2(1-|\Gamma_h|^2)\alpha + (1-|\Gamma_h|^2)} = \frac{\Delta_{max}-1}{\Delta_\infty - 1}. \tag{73}$$

The equation (73) is equivalent to the following second order equation:

$$\left(1 - \frac{\Delta_\infty - 1}{\Delta_{max} - 1}\right)\alpha^2 + 2(1-|\Gamma_h|^2)\alpha + (1-|\Gamma_h|^2) = 0, \tag{74}$$

which has a unique positive solution when $\Delta_\infty > \Delta_{max}$:

$$\alpha_0 = \frac{\left(1-|\Gamma_h|^2\right) + \sqrt{\left(1-|\Gamma_h|^2\right)\left(\frac{\Delta_\infty - 1}{\Delta_{max}-1} - |\Gamma_h|^2\right)}}{\frac{\Delta_\infty - 1}{\Delta_{max}-1} - 1}. \tag{75}$$

Appendix B: Received Power on the BS 2 with the RZF-CI Precoder

If $\Delta_\infty \leq \Delta_{max}$, then $\mathbf{w}_U = \mathbf{h}_U^H / \|\mathbf{h}_U\|$ and using (30), it comes:

$$\left|y_{BH}^U\right|^2 = P_U \left\|\mathbf{h}_U\right\|^2 \sigma_c^2. \tag{76}$$

If $\Delta_\infty > \Delta_{max}$, using (56) in (30), the received power on the BS 2 is equal to:

$$\begin{aligned} &\left|y_{BH}^U\right|^2 \\ &= P_U \sigma_c^2 \frac{\left|(1+\alpha_0)\left\|\mathbf{h}_U\right\| - |\Gamma_h|^2 \left\|\mathbf{h}_U\right\|\right|^2}{(1+\alpha_0)^2 - 2(1+\alpha_0)|\Gamma_h|^2 + |\Gamma_h|^2} \\ &= P_U \left\|\mathbf{h}_U\right\|^2 \sigma_c^2 \frac{\left((1+\alpha_0) - |\Gamma_h|^2\right)^2}{\left((1+\alpha_0) - |\Gamma_h|^2\right)^2 + |\Gamma_h|^2 - |\Gamma_h|^4}, \end{aligned} \tag{77}$$

and thus:

$$\begin{aligned} \left|y_{BH}^U\right|^2 &= P_U \left\|\mathbf{h}_U\right\|^2 \sigma_c^2 \\ &\times \left(1 - \frac{|\Gamma_h|^2\left(1-|\Gamma_h|^2\right)}{\left(1+\alpha_0-|\Gamma_h|^2\right)^2 + |\Gamma_h|^2\left(1-|\Gamma_h|^2\right)}\right). \end{aligned} \tag{78}$$

Finally, the received power on the BS 2 is equal to:

$$\left|y_{BH}^U\right|^2 = P_U \left\|\mathbf{h}_U\right\|^2 \sigma_c^2 \left(1 - \varepsilon.|\Gamma_h|^2\right), \tag{79}$$

with:

$$\begin{aligned} \varepsilon &= \left(\frac{\left(1+\alpha_0-|\Gamma_h|^2\right)^2}{1-|\Gamma_h|^2} + |\Gamma_h|^2\right)^{-1}, \\ &= \left(\left(1-|\Gamma_h|^2\right) + 2\alpha_0 + \frac{\alpha_0^2}{1-|\Gamma_h|^2} + |\Gamma_h|^2\right)^{-1}, \\ &= \left(1 + 2\alpha_0 + \frac{\alpha_0^2}{1-|\Gamma_h|^2}\right)^{-1}. \end{aligned} \tag{80}$$

As $\alpha_0 \geq 0$ and $|\Gamma_h|^2 \leq 1$, it comes $0 \leq \varepsilon \leq 1$.

Declarations

Ethics approval and consent to participate

Not applicable

Consent for publication

Not applicable

List of abbreviations

5G Fifth Generation of cellular networks

ARPU Average Revenue Per User

BER Bit Error Rate

BH BackHaul

BS Base Station

FDMA Frequency-Division Multiple Access
LOS Line-Of-Sight
MISO Multiple-Input Single-Output
mMIMO massive Multiple-Input Multiple-Output
MRT Maximum Ratio Transmission
MU-MIMO Multi-User Multiple-Input Multiple-Output
OFDM Orthogonal Frequency-Division Multiplexing
RMa Rural Macro-cell
RZF Regularized Zero Forcing
RZF-CI Regularized Zero Forcing with Controlled Interference
SDMA Space-Division Multiple Access
SINR Signal-to-Interference-plus-Noise Ratio
SNR Signal-to-Noise Ratio
TDD Time-Division Duplex
UE User Equipment
ZF Zero Forcing

Availability of data and material

The datasets supporting the conclusions of this article are included within the article and its additional files.

Competing interests

The authors declare that they have no competing interests.

Funding

This work has been performed in the framework of the Horizon 2020 project ONE5G (ICT-760809) receiving funds from the European Union.

Authors' contributions

Alexis Bazin, Bruno Jahan and Maryline Hélard have:

- made substantial contributions to conception and design, or acquisition of data, or analysis and interpretation of data;
- been involved in drafting the manuscript or revising it critically for important intellectual content;
- given final approval of the version to be published;
- participated sufficiently in the work to take public responsibility for appropriate portions of the content;
- agreed to be accountable for all aspects of the work in ensuring that questions related to the accuracy or integrity of any part of the work are appropriately investigated and resolved.

Acknowledgements

The authors would like to acknowledge the contributions of their colleagues in the project ONE5G (ICT-760809), although the views expressed in this contribution are those of the authors and do not necessarily represent the project.

Author details

[1]Department of Advanced Wireless Evolution, Orange Labs, 4 rue du Clos Courtel, 35512 Cesson-Sévigné, France. [2]Univ Rennes, INSA Rennes, CNRS, IETR (Institut d'Electronique et de Télécommunications de Rennes), UMR 6164, F-35000 Rennes, France.

References

1. ICT Facts and Figures 2017. Technical report, International Telecommunication Union (ITU). www.itu.int
2. Naveh, T.: Mobile Backhaul: Fiber vs. Microwaves. Case Study Analyzing Various Backhaul Technology Strategies. White Paper (October 2009)
3. Hur, S., Kim, T., Love, D.J., Krogmeier, J.V., Thomas, T.A., Ghosh, A.: Millimeter Wave Beamforming for Wireless Backhaul and Access in Small Cell Networks. IEEE Transactions on Communications **61**(10), 4391–4403 (2013). doi:10.1109/TCOMM.2013.090513.120848
4. Huurdeman, A.A.: Radio-relay Systems. The Artech House telecommunications library. Artech House, Boston (1995). OCLC: 832307035
5. Balachandran, K., Kang, J., Karakayali, K., Singh, J.: Capacity Benefits of Relays with In-Band Backhauling in Cellular Networks. In: 2008 IEEE International Conference on Communications, pp. 3736–3742 (2008). doi:10.1109/ICC.2008.702
6. Chia, S., Gasparroni, M., Brick, P.: The next challenge for cellular networks: backhaul. IEEE Microwave Magazine **10**(5), 54–66 (2009). doi:10.1109/MMM.2009.932832
7. Taori, R., Sridharan, A.: Point-to-multipoint in-band mmwave backhaul for 5g networks. IEEE Communications Magazine **53**(1), 195–201 (2015). doi:10.1109/MCOM.2015.7010534
8. Góra, J., Redana, S.: Resource management issues for multi-carrier relay-enhanced systems. EURASIP Journal on Wireless Communications and Networking **2012**, 124 (2012). doi:10.1186/1687-1499-2012-124. Accessed 2018-03-02
9. de Moraes, T.M., Nisar, M.D., Gonzalez, A.A., Seidel, E.: Resource allocation in relay enhanced LTE-Advanced networks. EURASIP Journal on Wireless Communications and Networking **2012**, 364 (2012). doi:10.1186/1687-1499-2012-364. Accessed 2018-03-02
10. Lagen, S., Agustin, A., Vidal, J.: Network-MIMO for downlink in-band relay transmissions. EURASIP Journal on Wireless Communications and Networking **2013**, 13 (2013). doi:10.1186/1687-1499-2013-13. Accessed 2018-03-02
11. Marzetta, T.L.: Noncooperative Cellular Wireless with Unlimited Numbers of Base Station Antennas. IEEE Transactions on Wireless Communications **9**(11), 3590–3600 (2010). doi:10.1109/TWC.2010.092810.091092
12. Larsson, E., Edfors, O., Tufvesson, F., Marzetta, T.: Massive MIMO for next generation wireless systems. IEEE Communications Magazine **52**(2), 186–195 (2014). doi:10.1109/MCOM.2014.6736761
13. Le, L.B., Lau, V., Jorswieck, E., Dao, N.-D., Haghighat, A., Kim, D.I., Le-Ngoc, T.: Enabling 5g mobile wireless technologies. EURASIP Journal on Wireless Communications and Networking **2015**, 218 (2015). doi:10.1186/s13638-015-0452-9. Accessed 2018-03-02
14. Björnson, E., Bengtsson, M., Ottersten, B.: Optimal Multiuser Transmit Beamforming: A Difficult Problem with a Simple Solution Structure [Lecture Notes]. IEEE Signal Processing Magazine **31**(4), 142–148 (2014). doi:10.1109/MSP.2014.2312183
15. El-Khamy, S.E., Moussa, K.H., El-Sherif, A.A.: C5. Performance

analysis of massive MIMO multiuser transmit beamforming techniques over generalized spatial channel model. In: Radio Science Conference (NRSC), 2015 32nd National, pp. 139–146 (2015). doi:10.1109/NRSC.2015.7117824

16. Ngo, H.Q., Larsson, E.G., Marzettat, T.L.: Uplink power efficiency of multiuser MIMO with very large antenna arrays. In: 2011 49th Annual Allerton Conference on Communication, Control, and Computing (Allerton), pp. 1272–1279 (2011). doi:10.1109/Allerton.2011.6120314
17. Ngo, H.Q., Larsson, E.G., Marzetta, T.L.: Energy and Spectral Efficiency of Very Large Multiuser MIMO Systems. IEEE Transactions on Communications **61**(4), 1436–1449 (2013). doi:10.1109/TCOMM.2013.020413.110848
18. Rusek, F., Persson, D., Lau, B.K., Larsson, E.G., Marzetta, T.L., Edfors, O., Tufvesson, F.: Scaling Up MIMO: Opportunities and Challenges with Very Large Arrays. IEEE Signal Processing Magazine **30**(1), 40–60 (2013). doi:10.1109/MSP.2011.2178495
19. Hoydis, J., ten Brink, S., Debbah, M.: Massive MIMO in the UL/DL of Cellular Networks: How Many Antennas Do We Need? IEEE Journal on Selected Areas in Communications **31**(2), 160–171 (2013). doi:10.1109/JSAC.2013.130205
20. Gao, Z., Dai, L., Mi, D., Wang, Z., Imran, M.A., Shakir, M.Z.: MmWave massive-MIMO-based wireless backhaul for the 5g ultra-dense network. IEEE Wireless Communications **22**(5), 13–21 (2015). doi:10.1109/MWC.2015.7306533
21. Li, B., Zhu, D., Liang, P.: Small Cell In-Band Wireless Backhaul in Massive MIMO Systems: A Cooperation of Next-Generation Techniques. IEEE Transactions on Wireless Communications **14**(12), 7057–7069 (2015). doi:10.1109/TWC.2015.2464299
22. Sanguinetti, L., Moustakas, A.L., Debbah, M.: Interference Management in 5g Reverse TDD HetNets With Wireless Backhaul: A Large System Analysis. IEEE Journal on Selected Areas in Communications **33**(6), 1187–1200 (2015). doi:10.1109/JSAC.2015.2416991
23. Tabassum, H., Sakr, A.H., Hossain, E.: Massive MIMO-Enabled Wireless Backhauls for Full-Duplex Small Cells. In: 2015 IEEE Global Communications Conference (GLOBECOM), pp. 1–6 (2015). doi:10.1109/GLOCOM.2015.7417670
24. Tabassum, H., Sakr, A.H., Hossain, E.: Analysis of Massive MIMO-Enabled Downlink Wireless Backhauling for Full-Duplex Small Cells. IEEE Transactions on Communications **64**(6), 2354–2369 (2016). doi:10.1109/TCOMM.2016.2555908
25. Vu, T.K., Bennis, M., Samarakoon, S., Debbah, M., Latva-aho, M.: Joint In-Band Backhauling and Interference Mitigation in 5g Heterogeneous Networks. In: European Wireless 2016; 22th European Wireless Conference, pp. 1–6 (2016)
26. Lo, T.K.Y.: Maximum ratio transmission. IEEE Transactions on Communications **47**(10), 1458–1461 (1999). doi:10.1109/26.795811
27. Peel, C.B., Hochwald, B.M., Swindlehurst, A.L.: A vector-perturbation technique for near-capacity multiantenna multiuser communication-part I: channel inversion and regularization. IEEE Transactions on Communications **53**(1), 195–202 (2005). doi:10.1109/TCOMM.2004.840638
28. Yu, K., Bengtsson, M., Ottersten, B., Beach, M.: Narrowband MIMO Channel Modeling for LOS Indoor Scenarios. In: DIVA (2002). http://urn.kb.se/resolve?urn=urn:nbn:se:kth:diva-46722 Accessed 2018-06-07
29. Cottatellucci, L., Debbah, M., Muller, R.R.: On the capacity of MIMO rice channels. 42nd Annual Allerton Conference on Communication, Control and Computing (2004). Accessed 2018-06-07
30. Sakaguchi, K., CHUA, H.-Y.-E., Araki, K.: MIMO channel capacity in an indoor Line-Of-Sight (LOS) environment. IEICE Transactions on Communications **E88B** (2005). doi:10.1093/ietcom/e88-b.7.3010
31. Boyd, S., Vandenberghe, L.: Convex Optimization. Cambridge University Press, Cambridge (2004). doi:10.1017/CBO9780511804441. http://ebooks.cambridge.org/ref/id/CBO9780511804441 Accessed 2018-06-18
32. Jaeckel, S., Raschkowski, L., Börner, K., Thiele, L.: QuaDRiGa: A 3-D Multi-Cell Channel Model With Time Evolution for Enabling Virtual Field Trials. IEEE Transactions on Antennas and Propagation **62**(6), 3242–3256 (2014). doi:10.1109/TAP.2014.2310220
33. Jaeckel, S., Raschkowski, L., Börner, K., Thiele, L., Burkhardt, F., Eberlein, E.: QuaDRiGa - Quasi Deterministic Radio Channel Generator, User Manual and Documentation. Tech. Rep. v1.4.8-571, Fraunhofer Heinrich Hertz Institute (2016)
34. Study on channel model for frequencies from 0.5 to 100 GHz. Technical Report TR 38.901, 3GPP. `www.3gpp.org`

Figures

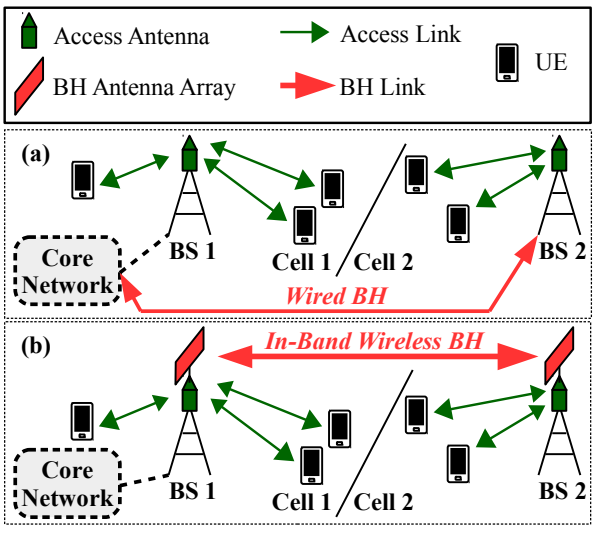

Figure 1 Scenario comparison between (a) a wired BH and (b) an in-band wireless BH.

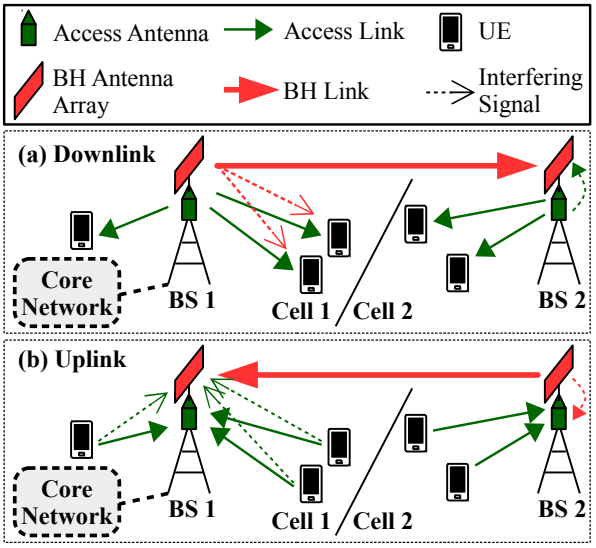

Figure 2 Description of (a) the downlink and (b) the uplink of the considered in-band wireless BH scenario.

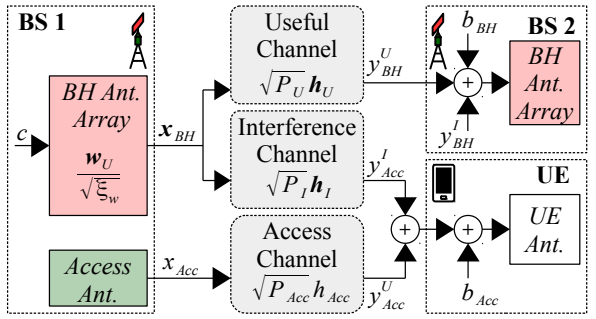

Figure 3 System model for an in-band wireless BH transmission.

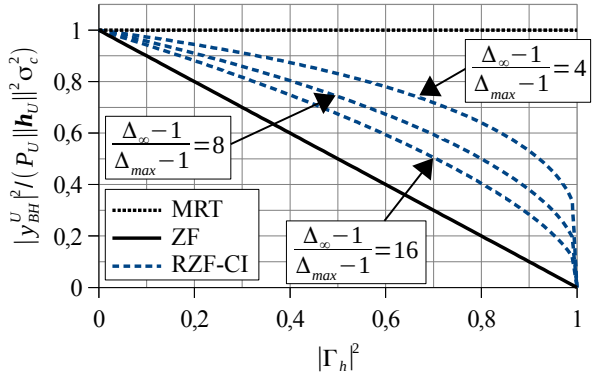

Figure 4 Theoretical normalized received useful power on the BH antenna array of the BS 2 as a function of the correlation factor Γ_h, for the three considered precoding techniques.

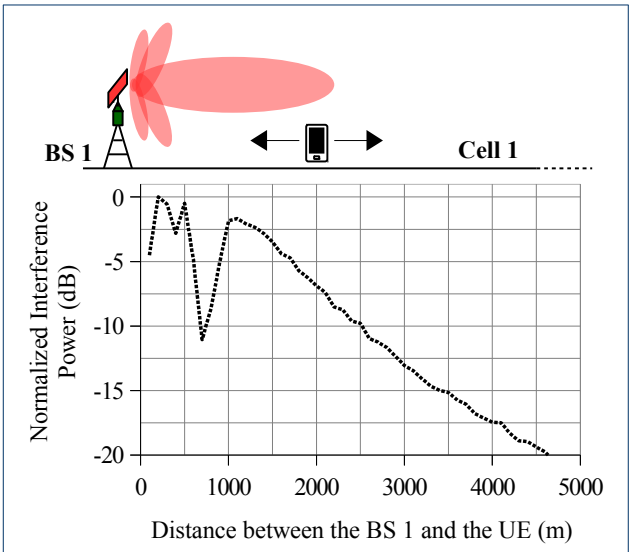

Figure 5 Normalized interference power on the UE side as a function of the distance between the BS 1 and the UE when the MRT precoder is used.

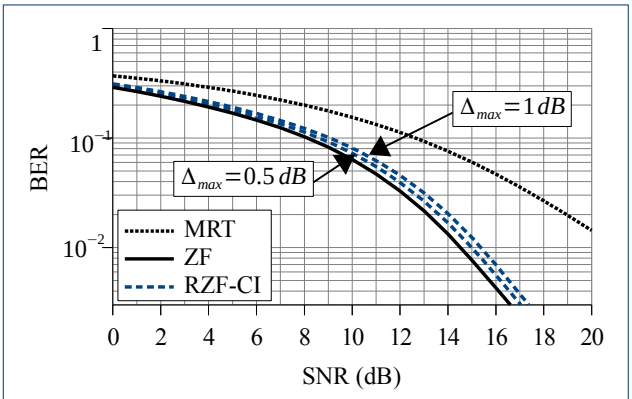

Figure 6 BER on the UE side as a function of the SNR for the three considered precoding techniques.

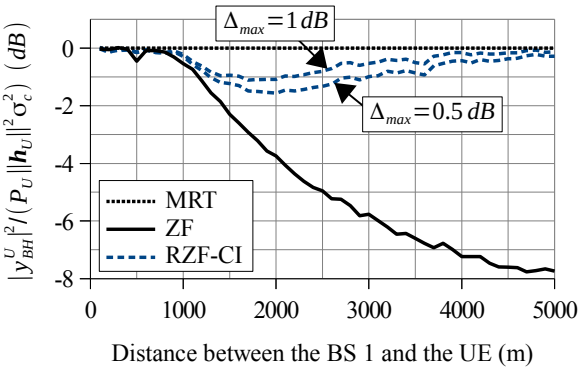

Figure 7 Normalized received useful power on the BH antenna array of the BS 2 as a function of the distance between the BS 1 and the UE for the three considered precoding techniques.